Heat Capacities of the $S = {}^1/_2$ Two-Dimensional Heisenberg Antiferromagnet Bis(2-amino-5-chloropyridinium) Tetrabromocuprate(II) $[(5CAP)_2CuBr_4]$ and Its Diamagnetic Analogue $[(5CAP)_2ZnBr_4]$[||]

Tetsuya Matsumoto,[†] Yuji Miyazaki,[†] Andrew S. Albrecht,[‡] Christopher P. Landee,*[,‡] Mark M. Turnbull,[§] and Michio Sorai*[,†]

Research Center for Molecular Thermodynamics, Graduate School of Science, Osaka University, Toyonaka, Osaka 560-0043, Japan, Department of Physics, Clark University, Worcester, Massachusetts 01610, and Carlson School of Chemistry, Clark University, Worcester, Massachusetts 01610

Received: June 2, 2000

Heat capacities of the spin quantum number $S = {}^1/_2$ two-dimensional Heisenberg antiferromagnet bis(2-amino-5-chloropyridinium) tetrabromocuprate(II) $[(5CAP)_2CuBr_4]$ crystal and its nonmagnetic analogue, the bis(2-amino-5-chloropyridinium) tetrabromozincate(II) $[(5CAP)_2ZnBr_4]$ crystal, were measured by adiabatic calorimetry. For the $(5CAP)_2ZnBr_4$ crystal, single-crystal X-ray diffraction was also performed. The $(5CAP)_2ZnBr_4$ crystal belongs to the orthorhombic space group *Pbca*, with $a = 16.074(2)$ Å, $b = 7.688(2)$ Å, $c = 30.538(6)$ Å, and $Z = 8$. In the $(5CAP)_2CuBr_4$ crystal, an antiferromagnetic phase transition occurred at $T_N = 5.08$ K, and a thermal anomaly arising from the short-range order characteristic of two-dimensional magnetic substances was found above T_N; the heat capacity of the $(5CAP)_2ZnBr_4$ crystal showed no thermal anomaly. The enthalpy and entropy gains due to the magnetic transition were estimated to be 49.3 J mol^{-1} and 5.65 J K^{-1} mol^{-1}, respectively. The value of the entropy gain coincides well with the R ln 2 (5.76 J K^{-1} mol^{-1}, R stands for the gas constant) expected for $S = {}^1/_2$ spin systems. The thermal anomaly observed above T_N is well accounted for in terms of the $S = {}^1/_2$ two-dimensional antiferromagneic Heisenberg model of a square lattice with $J/k_B = -4.3$ K. Spin wave analysis of the magnetic heat capacities below T_N suggests that the $(5CAP)_2CuBr_4$ crystal is in a three-dimensional antiferromagnetic state, which is realized by a weak interlayer magnetic interaction between the two-dimensional layers.

1. Introduction

In the last three decades, studies on low-dimensional magnetism have been devoted to the understanding of phase transitions and critical phenomena. The quantum effects of low-dimensional magnetic systems—for instance, Haldane's hypothesis concerning one-dimensional Heisenberg antiferromagnets,[1,2] the question of whether the resonating valence bond state is the ground state of spin quantum number $S = {}^1/_2$ Heisenberg antiferromagnets,[3−8] and so on—have also been currently debated topics. Recently, it has been pointed out that the low dimensionality of magnets is associated with the mechanism of superconductivity in some copper oxides.[9,10]

As for two-dimensional magnetism, it is well known that two-dimensional Ising spin systems give rise to a magnetic phase transition,[11] while ideal two-dimensional Heisenberg spin systems do not bring about any magnetic phase transitions.[12] However, actual two-dimensional magnetic substances exhibit a magnetic phase transition at low temperatures and lead to a three-dimensional magnetic ordering state due to the presence of weak Ising anisotropy, the existence of weak interlayer magnetic interaction between the two-dimensional magnetic layers, or both. This dimensional crossover often makes it difficult to realize ideal two-dimensional magnetic systems experimentally.

The catalog of known two-dimensional $S = {}^1/_2$ Heisenberg antiferromagnets is very small. Many more $S = {}^1/_2$ Heisenberg layers with intralayer ferromagnetic interactions have been investigated (K_2CuF_4 and $(C_nH_{2n+1}NH_3)_2CuX_4$, where X = Cl or Br).[13] While these compounds typically order as three-dimensional antiferromagnets due to a weak antiferromagnetic coupling between the layers, their behavior above the critical temperatures is dominated by the ferromagnetic sign of the intralayer interactions. In contrast, compounds in which the intralayer exchange is antiferromagnetic are fewer and have been less studied. The best known 2D antiferromagnet is La_2CuO_4,[14] a compound well studied as the insulating end member of the series of high-temperature superconductors $La_{2-x}Sr_xCuO_4$. It has an extremely large exchange constant ($J/k_B = 850$ K), which makes the investigation of field-dependent properties impossible. Other known antiferromagnetic copper layers include copper formate tetrahydrate, $Cu(HCOO)_2(H_2O)_4$,[15] and copper formate diureate dihydrate, $Cu(HCOO)_2{\cdot}2(NH_2)_2CO{\cdot}2H_2O$.[16] These compounds contain isolated layers of two inequivalent Cu(II) ions, each linked to four others by bridging formate ions. The layers in the tetrahydrate are separated by hydrogen-bonded water molecules, while the layers in the urea compound are further separated by the additional organic molecules. The intralayer exchange constants for the tetrahydrate and urea compounds have been found to be near 40 and 33 K,[16] respectively. Heat capacity studies have found the ordering temperatures to be at 16.5[17] and 15.5 K.[16] The existence of two inequivalent copper sites will lead to spin-canting, which breaks the high symmetry required for the Heisenberg model.

[||] Contribution No. 30 from the Research Center for Molecular Thermodynamics.

* Corresponding authors. [C.P.L.] Tel: +1-508-793-7439. Fax: +1-508-793-8861. E-mail: clandee@clarku.edu. [M.S.] Tel: +81-6-6850-5523. Fax: +81-6-6850-5526. E-mail: sorai@chem.sci.osaka-u.ac.jp.

[†] Research Center for Molecular Thermodynamics, Osaka University.

[‡] Department of Physics, Clark University.

[§] Carlson School of Chemistry, Clark University.

10.1021/jp0020081 CCC: $19.00
Published on Web 10/06/2000

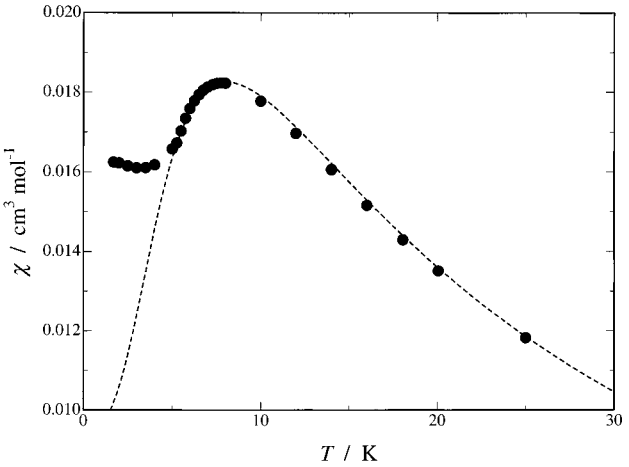

Figure 1. Magnetic susceptibility of $(5CAP)_2CuBr_4$. Broken curve indicates the theoretical value for the $S = {}^1/_2$ two-dimensional square planar Heisenberg antiferromagnet with the exchange parameter $J/k_B = -4.3$ K.[24]

Landee and his collaborators are endeavoring to expand the available examples of low-dimensional quantum antiferromagnets through the application of the principles of molecule-based magnetism.[18] They are focusing on copper compounds with uniform copper sites and exchange interactions weak enough to be overcome using available magnetic fields. They have paid attention to A_2CuX_4 (A = 5CAP (2-amino-5-chloropyridinium) or 5MAP (2-amino-5-methylpyridinium) and X = Cl or Br) as new candidates of insulating $S = {}^1/_2$ two-dimensional Heisenberg antiferromagnets. In this family, the oxidation state of copper ion is 2 with a d^9 electron configuration, producing one unpaired spin ($S = {}^1/_2$) and a nearly quenched orbital angular momentum ($g \approx 2.1$). Structural and magnetic studies have so far been conducted for $(5MAP)_2CuBr_4$,[19,20] $(5MAP)_2CuCl_4$,[19,21] $(5CAP)_2CuCl_4$,[21] and $(5CAP)_2CuBr_4$.[22]

In the present study, we focus on the magnetic property of $(5CAP)_2CuBr_4$. This complex has the same crystal structure as those of the other three analogues, $(5MAP)_2CuCl_4$,[19] $(5MAP)_2CuBr_4$,[19] and $(5CAP)_2CuCl_4$.[21] The crystal of $(5CAP)_2CuBr_4$ belongs to the monoclinic system with the space group $C2/c$: $a = 13.050(5)$ Å, $b = 8.769(3)$ Å, $c = 15.810(5)$ Å, $\beta = 94.31(3)°$, and $Z = 4$.[22] Within the unit cell, distorted $CuBr_4^{2-}$ tetrahedra with the mean Br−Cu−Br large angle $\bar{\theta} \approx 137°$ are embedded at the corners and center of the plane parallel to the *ab* plane and are related by *C* centering. Equivalent layers of $CuBr_4^{2-}$ tetrahedra are located one-half unit cell apart along the *c* axis. Each copper site is related to others in the adjacent layers by the *c* glide symmetry operation. Magnetic pathways within the layers are available between the tetrahedra related by *C* centering via Br···Br contacts (4.35 Å). Within each plane, each Cu atom is linked to its four nearest neighbors through identical magnetic pathways, forming an effective square planar lattice. On the other hand, Cu sites along the *c* axis are related by two identical Br···Br contacts (4.83 Å), which lead to the interlayer magnetic interaction, much weaker than the intralayer interaction because the magnetic interaction is known to decrease exponentially with increasing Br···Br distance.[23]

As shown in Figure 1, the magnetic susceptibility measurements of polycrystalline $(5CAP)_2CuBr_4$ reveal a broad maximum around 7 K, with a maximum value of 1.83×10^{-2} cm^3 mol^{-1}. The broad maximum is characteristic of a low-dimensional Heisenberg antiferromagnet, so the data were fit to a polynomial expression for the susceptibility of the $S = {}^1/_2$ two-dimensional Heisenberg antiferromagnet.[24] The polynomial is based on a high-temperature series expansion[25] plus more recent calculations for the susceptibility at lower temperatures.[26] The broken curve represents the best fit for the data >5.5 K with parameters $J/k_B = -4.3(1)$ K and $g = 2.11(1)$, where the spin Hamiltonian is assumed as follows:

$$\mathbf{H} = -2J\mathbf{S}_i\mathbf{S}_j \qquad (1)$$

It is noted in Figure 1 that the theoretical curve and the polycrystalline data diverge sharply near 5.1 K. As will be shown later in this paper, that temperature has been found by heat capacity studies to be the Néel temperature for $(5CAP)_2CuBr_4$, so the powder susceptibility data can determine the ordering temperature. The onset of long-range ordering is more clearly seen in single-crystal susceptibility studies of $(5CAP)_2CuBr_4$, as reported in ref 22.

Adiabatic heat capacity calorimetry is a crucially important tool for investigating the thermal properties of substances. Heat capacity is sensitive to a change in the degree of long-range and short-range ordering, so it may play a diagnostic role in determining the presence of magnetic phase transitions, which are sometimes difficult to detect solely by magnetic measurements. The main goal of the present paper is to elucidate whether a phase transition, if any, takes place in the present two-dimensional Heisenberg magnet and to examine the cause of the phase transition, either interlayer magnetic interaction or slight Ising character. To achieve this, we measured heat capacities of $(5CAP)_2CuBr_4$ and of its diamagnetic analogue, $(5CAP)_2ZnBr_4$, as a reference in determining the lattice heat capacity of $(5CAP)_2CuBr_4$. As a result, we clearly found a heat capacity peak at 5.08 K arising from the antiferromagnetic phase transition. This is caused by the dimensional crossover between the two-dimensional character at high temperatures and the three-dimensional character at low temperatures.

2. Experimental Section

A. Sample Preparation. Crystals of $(5CAP)_2CuBr_4$ were synthesized by slow evaporation of an aqueous solution of anhydrous $CuBr_2$ (2.23 g, 10 mmol), dilute (20%) HBr (8.1 g, 20 mmol), and 2-amino-5-chloropyridine (2.57 g, 20 mmol). On the other hand, crystals of $(5CAP)_2ZnBr_4$ were prepared by slow evaporation of an aqueous solution of anhydrous $ZnBr_2$ (4.50 g, 20 mmol), dilute (40%) HBr (8.1 g, 40 mmol), and 2-amino-5-chloropyridine (5.14 g, 40 mmol). These chemical reactions are as follows:

$$2(\text{2-amino-5-chloropyridine}) + MBr_2 + 2HBr \rightarrow (5CAP)_2MBr_4 \qquad M = Cu, Zn$$

The results of the elemental analyses for the obtained crystals are as follows. Calcd for $(5CAP)_2CuBr_4$ ($C_{10}H_{12}N_4Br_4Cl_2Cu$): C, 18.70; H, 1.88; N, 8.72. Found: C, 18.79; H, 1.80; N, 8.73. Calcd for $(5CAP)_2ZnBr_4$ ($C_{10}H_{12}N_4Br_4Cl_2Zn$): C, 18.65; H, 1.88; N, 8.70. Found: C, 18.65; H, 1.72; N, 8.72. The infrared spectra for the KBr pellet show significant absorptions at 3424(m), 3307(m), 1662(s), 1608(s), 1331(m), 820(m), and 661(m) cm^{-1} for $(5CAP)_2CuBr_4$ and at 3430(m), 3311(m), 1664(s), 1612(s), 1333(m), 833(m), and 670(m) cm^{-1} for $(5CAP)_2ZnBr_4$ (the letters s and m indicate strong and medium intensities, respectively).

B. Heat Capacity Measurement. Heat capacities of the samples were measured with two types of adiabatic calorimeters covering different temperature regions. In the 0.5−20 K temperature range, a very low-temperature adiabatic calorimeter workable with a ^{3}He/^{4}He dilution refrigerator[27] was employed. Polycrystalline samples of $(5CAP)_2CuBr_4$ and $(5CAP)_2ZnBr_4$ were formed onto disks 2 cm in diameter and loaded into a

TABLE 1: Crystal and Refinement Data for $(5CAP)_2ZnBr_4$[a]

chemical formula	$C_{10}H_{12}N_4Br_4Cl_2Zn$	formula weight	644.14
crystal system	orthorhombic	space group	*Pbca*
a (Å)	16.074(2)	*V* (Å^3)	3773.8(13)
b (Å)	7.688(2)	*Z*	8
c (Å)	30.538(6)		
crystal dimensions (mm^3)	0.6 × 0.3 × 0.2	ρ_{calcd} (g cm^{-3})	2.267
μ (mm^{-1})	10.052	λ (Å)	0.71073
θ_{min} (deg)	2.53	θ_{max} (deg)	22.85
unit cell reflections	3532	temperature (K)	293(2)
radiation type	Mo Kα	diffractometer	SMART CCD
total reflections	3532	reflections ≥ 2σ	3305
limits	$0 \le h \le 19$, $0 \le k \le 9$, $0 \le l \le 37$	*F*(000)	2432
structure solution	direct method (SHELXS97)	structure refinement	SHELXL97
refinement type	full-matrix least squares	parameters	190 (for all 3532 reflections)
R ($\|I\| = 2\sigma$)	0.0465	R (all data)	0.0514
R_w ($\|I\| = 2\sigma$)	0.0987	R_w (all data)	0.1012
goodness of fit	1.344	measured fraction of data	0.851
largest peak	0.674	largest hole	−0.869

[a] Refinement of F^2 against all reflections. The weighted R factor R_w and goodness of fit S are based on F^2; conventional R factors R are based on F, with F set to zero for negative F^2. The threshold expression of $F^2 \ge 2\sigma(F^2)$ is used only for calculating R factors (*gt*), etc., and is not relevant to the choice of reflections for refinement. R factors based on F^2 are statistically about twice as large as those based on F, and R factors based on all data will be even larger. Weighting scheme: $w = 1/[\sigma^2(F_o^2) + (0.0231P)^2 + 29.4964P]$, where $P = (F_o^2 + 2F_c^2)/3$.

TABLE 2: Selected Bond Lengths and Angles for $(5CAP)_2ZnBr_4$

atom 1	atom 2	length (Å)
Zn	Br1	2.4618(11)
Zn	Br2	2.3812(10)
Zn	Br3	2.4056(10)
Zn	Br4	2.3922(10)

atom 1	atom 2	atom 3	angle (deg)
Br1	Zn	Br2	110.49(4)
Br1	Zn	Br3	105.41(4)
Br1	Zn	Br4	104.96(4)
Br2	Zn	Br3	113.15(4)
Br2	Zn	Br4	110.37(4)
Br3	Zn	Br4	112.04(4)

gold-plated copper cell without any heat exchange medium. The masses of the disks were 1.50216 and 3.58022 g. On the other hand, in the higher temperature range (13−305 K), a low-temperature adiabatic calorimeter[28] was used for $(5CAP)_2CuBr_4$. The $(5CAP)_2CuBr_4$ crystal (mass, 6.4681 g) was loaded into a gold-coated copper cell together with 590 Torr of ^{4}He gas as a heat exchange medium. For $(5CAP)_2ZnBr_4$, a low-temperature adiabatic calorimeter for small samples[29] was employed in the 7−301 K temperature range. The $(5CAP)_2ZnBr_4$ crystal (2.91667 g) was loaded into a gold-plated copper cell and sealed in 1 atm of ^{4}He gas to facilitate thermal equilibration. Buoyancy correction for the sample masses was made by using the densities of 2.365 g cm^{-3} for $(5CAP)_2CuBr_4$[22] and 2.267 g cm^{-3} for $(5CAP)_2ZnBr_4$.

C. Single-Crystal X-ray Diffraction. Colorless crystals of $(5CAP)_2ZnBr_4$ were grown by slow evaporation from aqueous solution, and a crystal of 0.6 × 0.3 × 0.2 mm^3 was selected. All data collections were carried out at 293(2) K on a Siemens SMART CCD diffractometer[30] with Mo Kα radiation (λ = 0.71073 Å) and a graphite monochromator. The intensities of 3532 reflections were measured by using ϕ and ω scans (R_σ = 0.0183). The structure was solved by the direct method (SHELXS-97).[31] Full-matrix least-squares refinement (SHELXL-97)[31] after absorption correction (SADABS)[32] gave $R = 0.0465$ and $R_w = 0.0987$ for $|I| \ge \sigma$. The hydrogen atoms were refined via a riding model with fixed isotropic U's. An absorption coefficient of 10.052 mm^{-1} was calculated. Neutral scattering factors and anomalous dispersion corrections for non-hydrogen atoms were taken from Ibers and Hamilton.[33] Full crystallographic data, atomic coordinates, isotropic thermal parameters, bond lengths and angles, and anisotropic thermal parameters are given in Supporting Information.

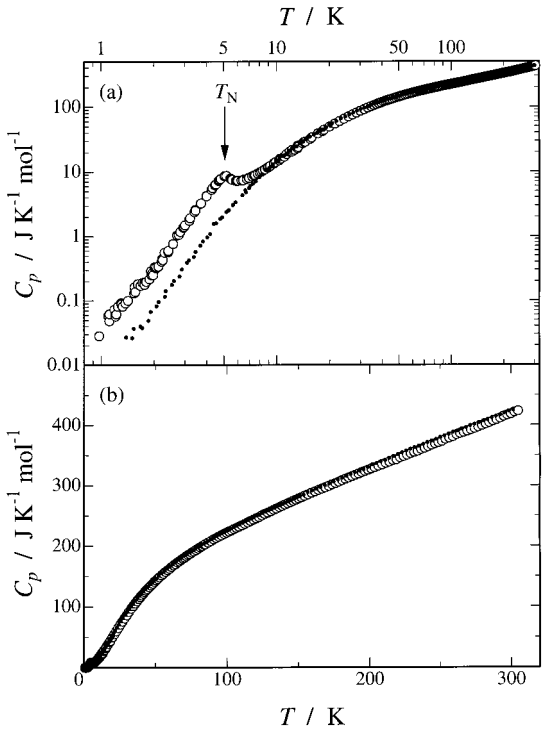

Figure 2. Molar heat capacities of $(5CAP)_2CuBr_4$ (○) and $(5CAP)_2ZnBr_4$ (●) crystals vs temperature on the (a) logarithmic and (b) normal scales.

3. Results and Discussion

A. Crystal Structure. X-ray crystal and refinement data of $(5CAP)_2ZnBr_4$ are given in Table 1. Bond lengths and angles for the Zn atom are given in Table 2. $(5CAP)_2ZnBr_4$ crystallizes in the orthorhombic space group *Pbca* with a = 16.074(2) Å, b = 7.688(2) Å, c = 30.538(6) Å, and Z = 8. The $ZnBr_4^{2-}$ ions are nearly tetrahedral with a mean trans angle of 112.6(1)°. The bond lengths and angles within the $5CAP^+$ ion are unremarkable. The $ZnBr_4^{2-}$ tetrahedra pack in the lattice without the uniform separation seen in $(5CAP)_2CuBr_4$.[22] The closest Br···Br contacts are 4.09(1) Å parallel to the b axis and 5.34(1) Å parallel to the c axis. Along the a axis, the distances alternate between 4.44(1) and 7.32(1) Å.

TABLE 3: Molar Heat Capacities of the $(5CAP)_2CuBr_4$ Crystal (M = 642.30 g Mol^{-1})[a]

T (K)	C_p (J K^{-1} mol^{-1})	T (K)	C_p (J K^{-1} mol^{-1})	T (K)	C_p (J K^{-1} mol^{-1})	T (K)	C_p (J K^{-1} mol^{-1})	T (K)	C_p (J K^{-1} mol^{-1})
series 1		11.10	17.09	series 5		198.85	325.5	31.64	91.63
1.117	0.0618	11.89	20.32	79.98	195.8	201.09	327.6	33.14	96.68
1.214	0.0567	12.74	21.94	82.63	199.7	203.51	329.7	34.59	101.3
1.312	0.0886			84.94	203.1	206.10	331.9	35.94	105.5
1.553	0.1631	series 3		86.91	205.7	208.69	334.0	37.21	109.3
1.942	0.2479	1.101	0.0583	88.84	208.3	211.26	336.5	38.41	112.9
2.065	0.3376	1.193	0.0730	90.74	210.8	213.82	338.7	39.54	116.2
2.233	0.4485	1.251	0.0812	92.61	213.3	216.38	341.2	40.63	119.0
2.418	0.5748	1.311	0.0867	94.45	215.6	218.92	342.8	41.66	121.8
2.832	1.174	1.380	0.0916	96.26	217.6	221.46	345.9	42.66	124.6
3.018	1.499	1.544	0.1316	98.04	220.0	223.98	348.0	43.62	127.1
3.220	1.919	1.620	0.1822	99.80	222.1	226.50	350.2	44.55	129.4
3.462	2.505	1.726	0.1917	101.54	224.0	229.00	352.6	45.66	132.3
3.719	3.246	1.767	0.1911	103.26	225.8	231.50	354.5	46.95	135.3
4.274	5.266	1.928	0.2889	104.96	227.9	233.99	356.8	48.19	138.1
4.527	6.396	2.023	0.3346	106.63	229.6	236.47	359.8	49.37	141.2
4.817	7.749	2.121	0.3423	108.51	231.9	238.94	361.7	50.52	143.5
5.185	8.628	2.248	0.4312	110.57	234.2	241.41	364.2	51.63	146.0
5.594	7.526	2.423	0.6017	112.61	236.5	243.87	366.6	52.87	148.8
6.022	7.252			114.63	238.8	246.32	369.0	54.31	151.9
6.464	7.544	series 4		116.62	241.1	248.76	371.0	55.75	154.7
6.940	8.072	0.976	0.0283	118.59	243.5	251.20	372.7	57.19	157.6
7.449	8.751	1.117	0.0484	120.55	245.6	253.70	376.5	58.58	160.4
8.033	9.771	1.206	0.0597	122.49	247.8	256.28	378.5	59.93	162.9
8.610	10.86	1.301	0.0923	124.49	250.5	258.86	380.7	61.31	165.5
9.203	12.26	1.425	0.1001	126.56	252.7	261.42	383.8	62.72	168.0
9.888	14.11	1.681	0.1714	128.61	254.9	263.98	386.2	64.10	170.5
10.62	15.99	1.775	0.1781	130.65	257.3	266.53	387.8	65.44	172.9
11.41	18.78	1.890	0.2172	132.67	259.5	269.07	389.7	66.75	175.0
12.25	20.48	1.983	0.2521	134.67	261.7	271.61	392.1	68.03	177.3
13.15	22.90	2.061	0.3212	136.66	263.9	274.18	394.4	69.29	179.4
14.10	27.37	2.215	0.4045	138.63	266.2	276.77	396.8	70.52	181.3
		2.579	0.7665	140.59	268.2	279.36	399.1	71.73	183.4
series 2		2.776	1.060	142.53	270.4	281.94	401.9	72.92	185.2
1.222	0.0616	2.980	1.410	144.47	272.4	284.52	403.9	74.13	187.0
1.330	0.0818	3.182	1.820	146.39	274.5	287.08	406.7	75.49	189.2
1.569	0.1372	3.411	2.383	148.30	276.3	289.64	408.9	76.93	191.3
1.809	0.1963	3.694	3.200	150.20	278.5	292.19	411.3	78.40	193.5
1.960	0.2683	4.002	4.259	152.08	280.2	294.73	414.3	79.92	195.8
2.303	0.5622	4.333	5.601	154.26	282.6	297.26	416.4	81.40	198.0
2.718	1.041	4.688	7.242	156.73	285.0	299.79	418.4	82.87	200.1
2.946	1.371	5.078	8.610	159.18	287.7	302.31	421.3	84.37	202.2
3.193	1.751	5.520	7.711	161.62	290.0	304.83	423.3		
3.454	2.585	5.989	7.186	164.04	292.4				
4.003	4.194	6.471	7.412	166.44	294.5	series 6			
4.475	6.187	6.991	7.994	168.83	296.7	13.30	24.18		
4.752	7.463	7.569	8.878	171.21	299.0	14.56	28.93		
5.065	8.553	8.210	10.02	173.58	301.5	15.85	33.86		
5.460	7.853	8.906	11.59	175.93	303.6	17.19	38.79		
5.881	7.227	9.665	13.51	178.27	306.0	18.56	43.92		
6.315	7.368	10.49	15.93	180.60	308.3	20.03	49.49		
6.781	7.740	12.29	21.73	182.91	310.6	21.50	54.94		
7.280	8.495	13.22	25.18	185.22	312.7	22.84	60.06		
7.813	9.407	14.34	28.73	187.51	315.1	24.22	65.28		
8.385	10.43	15.55	31.97	189.80	317.2	25.66	70.70		
8.997	11.81	18.26	42.13	192.08	319.3	27.07	75.81		
9.652	13.38			194.34	321.5	28.54	81.01		
10.35	15.06			196.60	323.5	30.07	86.27		

[a] Data in Series 1−6 were collected with different adiabatic calorimeters.

B. Heat Capacity. The molar heat capacities of the $(5CAP)_2CuBr_4$ crystal under constant pressure are listed in Table 3 and plotted in Figure 2. A heat capacity peak, which might be caused by three-dimensional antiferromagnetic ordering, was observed at 5.08 K. This corresponds to the temperature at which the magnetic susceptibility deviates from the theoretical curve.[24] Above the transition temperature, we found a large heat capacity tail due to the short-range ordering of a spin alignment characteristic of low-dimensional magnets, as expected from the structural analysis and the magnetic susceptibility measurement.[22,24]

The molar heat capacitites of the $(5CAP)_2ZnBr_4$ crystal are listed in Table 4 and plotted in Figure 2 together with those of the $(5CAP)_2CuBr_4$ crystal. No thermal anomaly was found over the temperature region studied. As expected from their molar masses, the heat capacities of the zinc complex are regularly larger than those of the copper complex except for in the magnetic thermal anomaly region.

C. Determination of Lattice and Magnetic Heat Capacities. We need to extract the magnetic contribution from the entire heat capacities of the sample to elucidate the magnetic properties. To achieve this, we must determine the lattice heat capacities. There are basically two ways for estimating the lattice heat capacities: one is to extrapolate a heat capacity curve by fitting smoothed functions (polynomial or Debye−Einstein functions) to the heat capacities in the temperature region of negligible contribution from the magnetic thermal anomaly, and the other is to approximate with the heat capacities of its nonmagnetic analogue.

TABLE 4: Molar Heat Capacities of the $(5CAP)_2ZnBr_4$ Crystal ($M = 644.14$ g mol^{-1})[a]

T (K)	C_p (J K^{-1} mol^{-1})	T (K)	C_p (J K^{-1} mol^{-1})	T (K)	C_p (J K^{-1} mol^{-1})	T (K)	C_p (J K^{-1} mol^{-1})
series 1		6.709	4.816	171.56	303.0	15.47	34.76
0.521	0.00125	7.322	6.512	174.57	306.1	16.32	37.95
0.897	0.00469	8.007	8.263	177.58	309.3	17.22	41.55
0.983	0.00661	8.753	10.64	180.59	312.2	18.11	44.99
		9.556	12.89	183.61	315.5	18.98	48.66
series 2		10.43	16.85	186.63	318.2	19.88	52.41
0.696	0.00360	11.41	19.12	189.64	321.2	20.75	55.81
0.853	0.00614	12.48	22.85	192.66	324.2	21.86	60.36
0.942	0.00478	13.65	27.52	195.68	326.1	23.24	65.86
1.039	0.00722	14.94	32.03	198.69	330.0	24.63	70.73
1.147	0.00917	16.33	37.25	201.70	334.2	26.02	76.35
1.390	0.0269	17.84	42.76	204.71	336.1	27.42	81.67
1.534	0.0367	19.14	47.78	207.73	339.4	28.83	86.69
1.719	0.0375	20.19	51.64	210.75	341.4	30.24	91.67
1.919	0.0673			213.77	345.1	31.67	96.09
2.129	0.0953	series 4		216.78	347.9	33.10	100.6
2.336	0.1405	80.73	200.3	219.80	350.7	34.54	105.1
2.601	0.2029	82.70	202.9	222.82	354.0	35.97	110.1
2.887	0.3074	84.69	205.4	225.83	356.9	37.41	114.4
3.171	0.4235	86.68	208.1	228.85	360.3	38.86	118.2
3.458	0.5737	88.67	210.8	231.86	362.7	40.31	122.2
3.809	0.8348	90.67	213.6	234.88	365.2	41.77	126.3
4.196	1.091	92.67	216.1	237.89	368.0	43.23	130.3
4.531	1.593	94.67	218.6	240.91	370.9	44.70	133.3
4.905	1.976	96.67	221.2	243.92	373.7	46.17	137.2
5.356	2.543	98.68	223.6	246.94	376.2	47.64	140.2
5.847	3.365	100.68	225.9	249.96	379.2	49.11	143.9
6.396	4.340	102.68	228.5	252.97	382.2	50.59	146.2
6.985	5.601	104.69	231.0	255.99	384.8	52.31	151.3
7.630	7.098	106.69	233.2	259.01	387.8	54.27	155.2
8.339	9.090	108.70	235.7	262.03	390.4	56.22	159.4
9.120	11.42	110.71	238.0	265.05	393.3	58.19	162.7
9.968	14.34	112.72	240.4	268.07	395.9	60.15	166.1
10.89	17.61	114.73	242.6	271.09	399.0	62.12	170.0
11.90	20.99	116.74	244.9	274.11	401.0	64.09	173.9
13.00	24.54	118.75	247.4	277.13	403.8	66.07	177.2
14.20	29.19	120.76	249.7	280.15	406.4	68.05	180.7
15.51	34.70	122.78	251.8	283.18	408.7	70.04	184.0
16.98	39.26	124.79	254.1	286.20	411.9	72.02	186.2
18.59	44.04	126.80	256.4	289.22	414.5	74.00	189.9
20.34	50.72	128.81	258.4	292.24	416.4	75.98	193.0
		130.83	260.8	295.27	419.7	77.97	195.5
series 3		132.84	262.8	298.29	422.7	79.96	198.8
1.507	0.0261	134.86	265.0	301.31	424.6	81.95	201.5
1.675	0.0399	136.88	267.1				
1.863	0.0488	138.89	269.1	series 5			
2.072	0.0819	140.90	271.2	6.653	5.169		
2.310	0.1152	142.92	273.3	7.074	6.070		
2.532	0.1765	144.93	275.4	7.613	7.356		
2.802	0.2383	146.95	277.6	8.193	8.904		
3.084	0.3900	148.97	280.1	8.852	10.76		
3.378	0.4791	150.98	281.7	9.564	12.96		
3.686	0.7141	153.49	284.2	10.32	15.13		
4.028	0.9629	156.50	288.7	11.14	17.99		
4.391	1.558	159.52	291.5	11.98	21.23		
4.779	1.865	162.52	293.9	12.85	24.53		
5.187	2.384	165.53	296.8	13.77	28.13		
5.645	3.047	168.54	300.0	14.65	31.48		

[a] Data in Series 1−5 were collected with different adiabatic calorimeters.

We first attempted the first way to determine the lattice heat capacities C_p(lattice) by using the temperature polynomial

$$C_p(\text{lattice}) = aT^3 + bT^5 + cT^7 + dT^9 \qquad (2)$$

Since the actual heat capacity C_p still involves a contribution from the short-range ordering of the spin alignment C_p(short-range) even far above the phase transition temperature, we assumed it to be approximated by the inverse square of temperature

$$C_p = C_p(\text{lattice}) + C_p(\text{short-range}) = aT^3 + bT^5 + cT^7 + dT^9 + eT^{-2} \qquad (3)$$

We fitted eq 3 to the observed heat capacity data between 7 and 25 K and obtained these values for the adjustable parameters: $a = 1.689 \times 10^{-2}$ J K^{-4} mol^{-1}, $b = -5.125 \times 10^{-5}$ J K^{-6} mol^{-1}, $c = 7.981 \times 10^{-8}$ J K^{-8} mol^{-1}, $d = -4.820 \times 10^{-11}$ J K^{-10} mol^{-1}, and $e = 165.7$ J K mol^{-1}. The lattice heat capacity curve thus estimated is drawn in Figure 3 with a dashed curve.

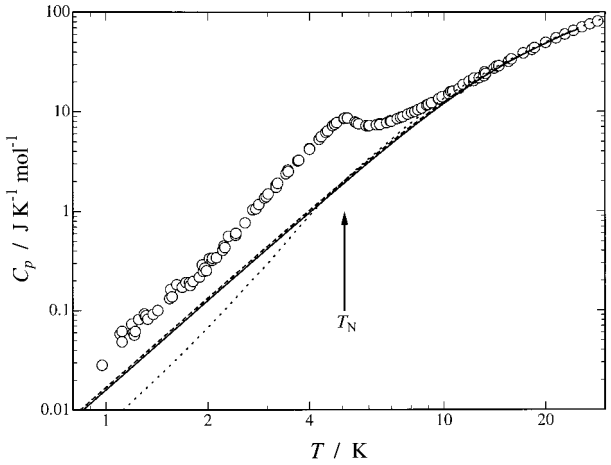

Figure 3. Molar heat capacities of the $(5CAP)_2CuBr_4$ crystal in the vicinity of the antiferromagnetic phase transition. Dashed, solid, and dotted curves indicate the lattice heat capacities derived from eqs 3 and 4 and the scaled heat capacities of $(5CAP)_2ZnBr_4$, respectively.

The magnetic heat capacities evaluated on the basis of this lattice heat capacity curve above the transition temperature were well accounted for in terms of the high-temperature series expansion of the $S = {}^1/_2$ two-dimensional antiferromagnetic Heisenberg model of a square lattice.[34] Therefore, to obtain a better fitting to the heat capacity data, we used the following equation in place of eq 3:

$$C_p = a'T^3 + b'T^5 + c'T^7 + d'T^9 + R\sum_{n=2}^{10}\frac{e_n}{2^n(n-2)!}\left(\frac{J}{k_BT}\right)^n \quad (4)$$

where R is the gas constant, J the exchange interaction parameter, k_B the Boltzmann constant, and e_n the coefficient of the $S = {}^1/_2$ two-dimensional Heisenberg model of a square lattice.[34] Equation 4 was fitted to the heat capacity data in the same temperature region (7−25 K) by adopting the Padé approximation. As expected, we obtained a better fitting when the parameters were $a' = 1.593 \times 10^{-2}$ J K^{-4} mol^{-1}, $b' = -4.478 \times 10^{-5}$ J K^{-6} mol^{-1}, $c' = 6.524 \times 10^{-8}$ J K^{-8} mol^{-1}, $d' = -3.739 \times 10^{-11}$ J K^{-10} mol^{-1}, and $J/k_B = -4.3$ K. The derived lattice heat capacity curve is shown in Figure 3 with a solid curve. The two lattice heat capacity curves derived from eqs 3 and 4 resemble each other.

Next, we tried the second way of determining the lattice heat capacities. We adopted $(5CAP)_2ZnBr_4$ as the nonmagnetic analogue because the relative atomic mass of Cu (63.55) is very close to that of Zn (65.39), although the crystal structures are different between the Cu compound (monoclinic $C2/c$)[22] and the Zn compound (orthorhombic *Pbca*). As shown in Figure 2, the heat capacities of $(5CAP)_2ZnBr_4$ are somewhat larger than those of $(5CAP)_2CuBr_4$ at temperatures where there is no thermal anomaly. This slight difference would originate from their different molecular masses and crystal structures. Then we modified the heat capacity of $(5CAP)_2ZnBr_4$ by multiplying the temperature by a factor of f to minimize the difference between this modification and the heat capacity of $(5CAP)_2CuBr_4$. We estimated f as 0.9745 by comparing the two sets of heat capacities at >50 K. The lattice heat capacity curve thus derived is drawn in Figure 3 with a dotted curve. This lattice heat capacity curve agrees well with the other two lattice heat capacity curves at >20 K, whereas it deviates somewhat from the others at <20 K. This deviation would be caused by the difference of the lattice vibration in the low-frequency region between $(5CAP)_2CuBr_4$ and $(5CAP)_2ZnBr_4$, which cannot be treated by a simple Debye model. Therefore, the method employing the heat capacities of a nonmagnetic analogue as the lattice heat capacities is not appropriate for the present case. Consequently, we adopted the lattice heat capacity curve estimated from eq 4.

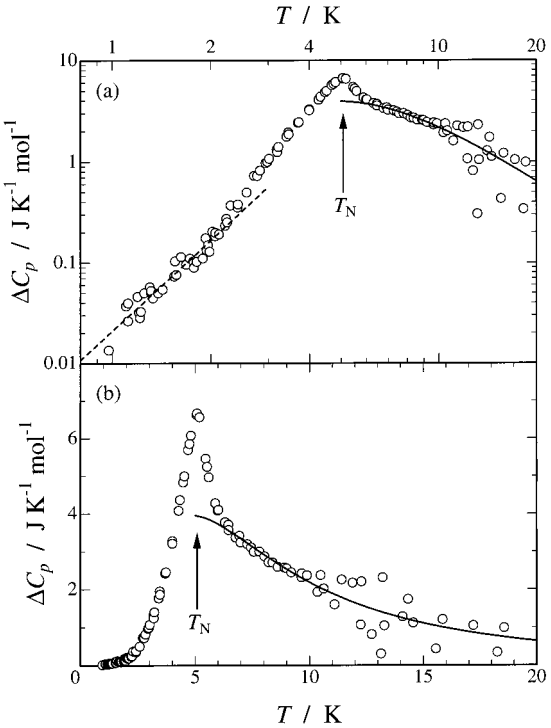

Figure 4. Magnetic heat capacities of the $(5CAP)_2CuBr_4$ crystal as a function of temperature on the (a) logarithmic and (b) normal scales. Solid curves indicate theoretical heat capacities for the $S = {}^1/_2$ two-dimensional antiferromagnetic Heisenberg model of a square lattice with $J/k_B = -4.3$ K. The broken line shows the heat capacity in accordance with the spin wave theory for the three-dimensional antiferromagnet.

The magnetic heat capacities of the sample were obtained by subtracting the lattice heat capacities from the observed heat capacities. They are shownagainst temperature in Figure 4. The heat capacity tail due to the short-range ordering of the two-dimensional spin system can be seen more clearly above the transition temperature.

D. Transition Enthalpy and Entropy. We can evaluate the enthalpy and entropy acquisitions due to the magnetic ordering by integration of the magnetic heat capacities ΔC_p with respect to T and ln T. The extrapolation of ΔC_p down to 0 K was performed using the spin wave theory, which is mentioned below in detail. On the other hand, the extrapolation of ΔC_p up to infinite temperature was performed using the high-temperature series expansion of the $S = {}^1/_2$ two-dimensional Heisenberg antiferromagnet of a square lattice.[34] The transition enthalpy and entropy thus evaluated are 49.3 J mol^{-1} and 5.65 J K^{-1} mol^{-1}, respectively.

The experimental transition entropy of 5.65 J K^{-1} mol^{-1} agrees well with the R ln 2 value (5.76 J K^{-1} mol^{-1}) expected for $S = {}^1/_2$ spin systems. This fact implies that the observed phase transition is indeed attributed to the magnetic ordering due to the $S = {}^1/_2$ spin in Cu^{2+} ions.

E. Mechanism of the Antiferromagnetic Phase Transition. The single-crystal X-ray diffraction study[22] of $(5CAP)_2CuBr_4$ indicated that this crystal contains two-dimensional planes made up of $S = {}^1/_2$ Cu^{2+} ions and Br^- ions. These planes are separated by $5CAP^+$ ions. Magnetic study[24] also revealed that the temperature dependence of the magnetic susceptibility is well reproduced by a pure $S = {}^1/_2$ two-dimensional antiferromagnetic

Heisenberg model. In fact, the heat capacity anomaly due to the short-range ordering effect can be well accounted for in terms of the $S = {}^1/_2$ two-dimensional antiferromagneic Heisenberg model of a square lattice[34] with $J/k_B = -4.3$ K. This value is in excellent agreement with $J/k_B = -4.3(1)$ K, obtained from the magnetic susceptibility measurement.[24] The theoretical heat capacity based on this model is shown in Figure 4 with solid curves. On the other hand, the present heat capacity measurement definitely revealed that the crystal regarded as the two-dimensional Heisenberg antiferromagnet undergoes an antiferromagnetic phase transition at $T_N = 5.08$ K. As far as we adopt the currently accepted theory that two-dimensional pure Heisenberg systems would not bring about phase transitions arising from the spin ordering,[12] the presence of the phase transition at 5.08 K implies that there exists a weak but definite magnetic interaction between the layers, leading to the so-called "dimensional crossover".

To estimate the interlayer magnetic interaction, we applied spin wave theory to the magnetic heat capacities below T_N. This theory is a good approximation for description of the low-temperature nature of magnetic substances. The low-temperature heat capacity due to the spin wave excitation, C_{SW}, is represented by the equation[13]

$$C_{SW} \propto T^{d/n} \tag{5}$$

where d stands for the dimensionality of the magnetic lattice and n is defined as the exponent in the dispersion relation: $n = 1$ for antiferromagnets and $n = 2$ for ferromagnets. We fitted the following expression to the magnetic heat capacities in the temperature range from 0.9 to 2.3 K

$$\Delta C_p = AT^{\alpha} \tag{6}$$

and obtained $\alpha = 2.98 \approx 3$. This result suggests that the spins in $(5CAP)_2CuBr_4$ crystal order into a three-dimensional antiferromagnet below the transition temperature. Hence we fitted eq 6 again with $\alpha = 3$ to the magnetic heat capacities in the same temperature region and obtained $A = 2.09 \times 10^{-2}$ J K^{-4} mol^{-1}. The spin wave heat capacity thus determined is drawn in Figure 4 with a broken line.

The spin wave heat capacity C_{SW} in a three-dimensional antiferromagnet possessing nonequivalent spin−spin interaction paths is expressed by either of the expressions[35]

$$C_{SW} = \frac{R\zeta(4)\Gamma(4)k_B{}^3}{16\pi^2 S^3 |J_1 J_2 J_3|^{1/2} |J_1 + J_2 + J_3|^{3/2}} T^3 \qquad J_1 < 0, J_2 < 0, J_3 < 0 \tag{7a}$$

$$C_{SW} = \frac{R\zeta(4)\Gamma(4)k_B{}^3}{16\pi^2 S^3 (J_1 J_2 J_3)^{1/2} |J_1 + J_2|^{3/2}} T^3 \qquad J_1 < 0, J_2 < 0, J_3 > 0 \tag{7b}$$

$$C_{SW} = \frac{R\zeta(4)\Gamma(4)k_B{}^3}{16\pi^2 S^3 (J_1 J_2)^{1/2} J_3{}^2} T^3 \qquad J_1 > 0, J_2 > 0, J_3 < 0 \tag{7c}$$

where J_1, J_2, and J_3 denote the exchange interaction parameters for three directions, ζ is Riemann's zeta function, Γ is Euler's gamma function, and S stands for the spin quantum number. Since the two-dimensional sheets of $CuBr_4{}^{2-}$ can be well approximated by a two-dimensional square lattice with two equivalent exchange interactions J, either eq 7a or 7b is applicable to the present crystal. If the interlayer interaction between the two sheets is expressed as J', eqs 7a and 7b can be rewritten as follows:

$$C_{SW} = \frac{R\zeta(4)\Gamma(4)k_B{}^3}{16\pi^2 S^3 |J| |J'|^{1/2} |2J + J'|^{3/2}} T^3 \qquad J < 0, J' < 0 \tag{8a}$$

$$C_{SW} = \frac{R\zeta(4)\Gamma(4)k_B{}^3}{32\sqrt{2}\pi^2 S^3 |J|^{5/2} J'^{1/2}} T^3 \qquad J < 0, J' > 0 \tag{8b}$$

Substituting $J/k_B = -4.3$ K into eqs 8a and 8b and comparing them with eq 6, we obtained $J'/k_B = -1.0$ K from eqs 6 and 8a and $J'/k_B = 1.4$ K from eqs 6 and 8b. In this analysis, we could not determine whether the interlayer interaction is ferromagnetic or antiferromagnetic, but the absolute value of J' is reliable in any case, considering the tendency that the magnetic interaction decreases exponentially with Br···Br distance.[23]

Acknowledgment. This study was partially supported by a grant-in-aid for scientific research on the priority areas of "metal-assembled complexes" (Area No. 401/12023229) from the Ministry of Education, Science, Sports and Culture, Japan.

Supporting Information Available: Complete tables of atom coordinates, bond lengths and angles, and equivalent isotropic and anisotropic thermal parameters. This material is available free of charge via the Internet at http://pubs.acs.org.

Appendix

Standard Thermodynamic Functions. The standard molar heat capacities, enthalpies, entropies, and Gibbs energies at

TABLE 5: Molar Standard Thermodynamic Functions of the $(5CAP)_2CuBr_4$ Crystal ($M = 642.30$ g mol^{-1})

T (K)	C_p° (J K^{-1} mol^{-1})	$(H_T^\circ - H_0^\circ)/T$ (J K^{-1} mol^{-1})	$S_T^\circ - S_0^\circ$ (J K^{-1} mol^{-1})	$-(G_T^\circ - H_0^\circ)/T$ (J K^{-1} mol^{-1})
1	0.0340	0.0107	0.0143	0.00359
2	0.2878	0.0732	0.0994	0.0262
5	8.343	1.989	2.544	0.5559
10	14.34	5.794	8.949	3.155
15	30.28	11.21	17.65	6.437
20	49.39	18.34	28.96	10.62
25	68.23	26.46	42.01	15.54
30	86.03	34.90	56.04	21.13
35	102.6	43.42	70.56	27.14
40	117.4	51.75	85.24	33.49
45	130.6	59.79	99.84	40.05
50	142.5	67.47	114.2	46.75
60	163.0	81.72	142.1	60.34
70	180.5	94.62	168.5	73.92
80	195.8	106.3	193.7	87.33
90	209.8	117.1	217.6	100.5
100	222.4	127.0	240.3	113.3
110	233.5	136.2	262.0	125.9
120	245.0	144.8	282.8	138.1
130	256.6	152.9	302.9	150.0
140	267.6	160.7	322.3	161.6
150	278.3	168.2	341.2	173.0
160	288.5	175.4	359.4	184.1
170	297.8	182.3	377.2	194.9
180	307.7	189.0	394.5	205.5
190	317.4	195.5	411.4	215.9
200	326.6	201.8	427.9	226.1
210	335.3	208.0	444.1	236.1
220	344.1	214.0	459.9	245.9
230	353.4	219.8	475.4	255.5
240	362.8	225.6	490.6	265.0
250	371.9	231.3	505.6	274.3
260	382.1	236.9	520.4	283.5
270	390.6	242.4	535.0	292.6
273.15	393.5	244.2	539.6	295.4
280	399.8	247.9	549.4	301.5
290	409.2	253.3	563.6	310.3
298.15	417.1	257.7	575.0	317.4
300	418.7	258.7	577.6	319.0

TABLE 6: Molar Standard Thermodynamic Functions of the $(5CAP)_2ZnBr_4$ Crystal ($M = 644.14$ g mol^{-1})

T (K)	C_p° (J K^{-1} mol^{-1})	$(H_T^\circ - H_0^\circ)/T$ (J K^{-1} mol^{-1})	$S_T^\circ - S_0^\circ$ (J K^{-1} mol^{-1})	$-(G_T^\circ - H_0^\circ)/T$ (J K^{-1} mol^{-1})
1	0.00679	0.00212	0.00288	0.000759
2	0.0751	0.0171	0.0227	0.00559
5	2.113	0.4773	0.6068	0.1296
10	14.41	3.925	5.233	1.308
15	32.36	10.37	14.42	4.047
20	52.11	18.27	26.36	8.092
25	72.24	27.14	40.23	13.09
30	90.81	36.24	55.08	18.84
35	106.7	45.17	70.27	25.10
40	121.4	53.82	85.52	31.70
45	134.1	62.07	100.6	38.52
50	145.3	69.86	115.3	45.46
60	165.8	84.28	143.8	59.50
70	183.9	97.26	170.8	73.49
80	198.8	109.0	196.3	87.26
90	212.6	119.8	220.5	100.7
100	225.1	129.7	243.6	113.9
110	237.2	138.9	265.6	126.7
120	248.8	147.6	286.7	139.1
130	259.8	155.8	307.1	151.3
140	270.2	163.6	326.7	163.1
150	280.9	171.1	345.7	174.6
160	291.9	178.3	364.2	185.9
170	301.5	185.2	382.2	196.9
180	311.6	192.0	399.7	207.7
190	321.6	198.5	416.8	218.3
200	331.8	204.9	433.5	228.6
210	340.9	211.2	450.0	238.8
220	350.9	217.3	466.1	248.7
230	361.2	223.4	481.9	258.5
240	370.0	229.3	497.4	268.2
250	379.3	235.1	512.7	277.6
260	388.7	240.8	527.8	287.0
270	397.9	246.5	542.6	296.2
273.15	400.4	248.2	547.3	299.0
280	406.2	252.0	557.3	305.2
290	415.0	257.5	571.7	314.2
298.15	422.6	261.9	583.3	321.4
300	423.8	262.9	585.9	323.0

rounded temperatures for the $(5CAP)_2CuBr_4$ and $(5CAP)_2ZnBr_4$ crystals were calculated from their experimental heat capacity data and are summarized in Tables 5 and 6. Extrapolation down to 0 K was performed by using the following odd-order polynomial functions:

$$C_p\,(\mathrm{J\,K^{-1}\,mol^{-1}}) = 4.606 \times 10^{-2}(T/\mathrm{K})^3 - 6.444 \times 10^{-3}(T/\mathrm{K})^5 + 9.896 \times 10^{-4}(T/\mathrm{K})^7 \quad (9)$$

for the $(5CAP)_2CuBr_4$ crystal and

$$C_p\,(\mathrm{J\,K^{-1}\,mol^{-1}}) = 7.010 \times 10^{-3}(T/\mathrm{K})^3 + 4.813 \times 10^{-4}(T/\mathrm{K})^5 + 1.728 \times 10^{-5}(T/\mathrm{K})^7 \quad (10)$$

for the $(5CAP)_2ZnBr_4$ crystal.

References and Notes

(1) Haldane, F. D. M. *Phys. Lett.* **1983**, *93A*, 464.
(2) Haldane, F. D. M. *Phys. Rev. Lett.* **1983**, *50*, 1153.
(3) Anderson, P. W. *Mater. Res. Bull.* **1973**, *8*, 153.
(4) Fazekas, P.; Anderson, P. W. *Philos. Mag.* **1974**, *30*, 423.
(5) Inoue, M.; Chikyu, T.; Hu, X.; Suzuki, M. *J. Phys. Soc. Jpn.* **1988**, *57*, 3733.
(6) Johnson, M. D.; Subbaswamy, K. R. *Phys. Rev. B* **1988**, *37*, 9390.
(7) Hamada, T.; Kane, J.; Nakagawa, S.; Natsume, Y. *J. Phys. Soc. Jpn.* **1988**, *57*, 1891.
(8) Natsume, Y.; Hamada, T.; Nakagawa, S.; Kane, J. *J. Phys. Soc. Jpn.* **1989**, *58*, 3869.
(9) Anderson, P. W.; Baskaran, G.; Zou, Z.; Hsu, T. *Phys. Rev. Lett.* **1987**, *58*, 2790.
(10) Anderson, P. W. *Science* **1987**, *235*, 1196.
(11) Onsager, L. *Phys. Rev.* **1944**, *65*, 117.
(12) Mermin, N. D.; Wagner, H. *Phys. Rev. Lett.* **1966**, *17*, 1133.
(13) de Jongh, L. J.; Miedema, A. R. *Adv. Phys.* **1974**, *23*, 1.
(14) Endoh, Y.; Yamada, K.; Birgeneau, R. J. *Phys. Rev. B* **1988**, *37*, 7443.
(15) Koyama, K.; Nobumasa, H.; Matsuura, M. *J. Phys. Soc. Jpn.* **1987**, *56*, 1553.
(16) Yamamoto, Y.; Matsuura, M.; Haseda, T. *J. Phys. Soc. Jpn.* **1976**, *40*, 1300.
(17) Yamamoto, Y.; Matsuura, M.; Haseda, T. *J. Phys. Soc. Jpn.* **1975**, *38*, 1776.
(18) Kahn, O. *Molecular Magnetism*; VCH: New York, 1993.
(19) Place, H.; Willett, R. D. *Acta Crystallogr. C* **1987**, *43*, 1050.
(20) Zhou, P.; Drumheller, J. E.; Rubenacker, G. V.; Halvorson, K.; Willett, R. D. *J. Appl. Phys.* **1991**, *69*, 5804.
(21) Hammer, P. R.; Dender, D. C.; Reich, D. H.; Albrecht, A. S.; Landee, C. P. *J. Appl. Phys.* **1997**, *81*, 4615.
(22) Giantsidis, J.; Turnbull, M. M.; Woodward, F. W.; Wynn, C. M.; Landee, C. P. Manuscript to be submitted to *Inorg. Chem.*
(23) Willett, R. D.; Place, H.; Middleton, M. *J. Am. Chem. Soc.* **1988**, *110*, 8639.
(24) Woodward, F. W.; Albrecht, A. S.; Wynn, C. M.; Landee, C. P.; Turnbull, M. M. Manuscript to be submitted to *Phys. Rev. B.*
(25) Navarro, R. In *Magnetic Properties of Layered Transition Metal Compounds*; de John, L. J., Ed.; Kluwer Academic Publishers: Dordrecht, The Netherlands, 1990; p 105.
(26) Kim, J. K.; Troyer, M. *Phys. Rev. Lett.* **1998**, *80*, 2705.
(27) Murakawa, S.; Wakamatsu, T.; Nakano, M.; Sorai, M.; Suga, H. *J. Chem. Thermodyn.* **1987**, *19*, 1275.
(28) Nishimori, A.; Nagano, Y.; Sorai, M. Unpublished results, Osaka University, Osaka, Japan, 1985.
(29) Kume, Y.; Miyazaki, Y.; Matsuo, T.; Suga, H. *J. Phys. Chem. Solids* **1992**, *53*, 1297.
(30) Data collection: *SMART* (1996). Cell refinement and data reduction: *SAINT* (1996). *SMART* and *SAINT*; Siemens Analytical X-Ray Instruments: Madison, WI.
(31) Sheldrick, G. M. *SHELXS97* and *SHELXL97*; University of Göttingen: Göttingen, Germany, 1997.
(32) Sheldrick, G. M. *SADABS*; University of Göttingen: Göttingen, Germany, 1996.
(33) In *International Tables for Crystallography*; Ibers, J. A., Hamilton, W. C., Eds.; Kynoch Press: Birmingham, AL, 1992; Vol. C.
(34) Baker, G. A., Jr.; Gilbert, H. E.; Eve, J.; Rushbrooke, G. S. *Phys. Lett.* **1967**, *25A*, 207.
(35) Ohmae, N.; Kajiwara, A.; Miyazaki, Y.; Kamachi, M.; Sorai, M. *Thermochim. Acta* **1995**, *267*, 435.